2018

Analysis of Water Evaporation in Twin Screw Compressors using Eulerian Multiphase Approach in CFD

Sham Ramchandra Rane
Centre for Compressor Technology, City University London, United Kingdom, sham.rane@city.ac.uk

Ahmed Kovacevic
a.kovacevic@city.ac.uk

Nikola Stosic
City University London, United Kingdom, n.stosic@city.ac.uk

Graham Stupple
Jäcklin GmbH, Germany, Stupple@jaecklin.de

Analysis of Water Evaporation in Twin Screw Compressors using Eulerian Multiphase Approach in CFD

Sham RANE*[1,3], Ahmed KOVAČEVIĆ[1], Nikola STOŠIĆ[1], Graham STUPPLE[2]

[1]Centre for Compressor Technology, City, University of London, EC1V 0HB, United Kingdom
[2]Jäcklin GmbH, Unterer Talweg 50, 86179 Augsburg, Germany
[3]University of Oxford, Department of Engineering Science, Oxford, OX2 0ES, United Kingdom

* Corresponding Author
sham.rane@city.ac.uk

ABSTRACT

3D CFD modelling is widely employed for the detailed analysis of flow and thermodynamics in complex machines such as twin screw compressors. The advantage of such high resolution simulations is that realistic geometry of the rotors and the ports can be captured. Additionally, the physical effects of fluid thermal interactions and leakage are directly captured by these models. Recent studies have shown that for dry air and oil injected air compressors a good agreement is achieved with measurements, in prediction of performance parameters. In these simulations the Eulerian-Eulerian multiphase modelling has been applied. To implement the same model for water injected compressors presents an additional challenge as the liquid water injected into the compression chamber changes phase and evaporates depending on the local saturation and thermodynamic conditions. Water also forms liquid film on the rotors and housing and thereby influences thermal changes.
In this paper a CFD model for water injected twin screw compressor that accounts for evaporation effects has been presented. Empirical form of the Lee evaporation-condensation model for phase change has been applied in the compression chamber using the phase specific mass and energy sources. Calculation of the amount of water required to just saturate the compressed air at delivery pressure is used to set the mass flow rate of water at two operating speeds. The effect of the suction air temperature and relative humidity is studied. Evaporation inside compression chamber has two important physical effects, one is that the latent heat of evaporating water lowers the gas temperature and the other is the change of state from water to vapour. Including vapour as a third phase in the CFD model adds a complexity to already challenging deforming grids required for twin screw domains. Hence a mass and energy source formulation is proposed in the presented study to account for the vapour phase and evaporation effects, thus limiting the number of phases to be modelled. Local drop in gas temperature, distribution of water and regions of evaporation were identified by the simulations. Thermal hot spots on the rotor were located. Reduction in the leakage of gas and its exit temperature was well predicted by the model. Such simplified evaporation model can be further used in the design of water injected screw compressors and extended to predict thermal deformation of the rotors and the housing.

1. INTRODUCTION

The idea of injecting liquid water in twin screw air compressors has been utilised for long time due to the thermodynamic benefits that supersede a dry air compression process (Stosic et al, 2004). There are industrial processes requiring clean compressed air where oil contamination is not acceptable such as in the food and pharmaceutical plants. In the absence of oil in the compression chamber, leakage and thermal deformations pose limits on the delivery pressures that could be achieved in one compression stage. As such, the multistage compression with intercooling has been employed which adds immensely to the cost of the compressor plant. When water is used in small quantities during the compression process an internal cooling and sealing can be achieved and also a condenser fitted downstream of the compressor can strain the water out of delivered high pressure air. In such a system or when there are no condensers employed it is desirable to inject an optimum quantity of water into the compression chamber in order to establish evaporative cooling. Twin screw compressors with water injection are also used to supply clean compressed air for the Proton Exchange Membrane (PEM) fuel cell systems. Humidity and temperature of the inlet air must be kept at desirable levels to achieve optimum fuel cell performance. Ous et al (2012), have reported experimental investigation of water injection in Twin Screw compressors in order to achieve humidification and cooling for fuel cell stacks. The effect on humidity due to injection was higher at low operating speeds and air mass

flow rates (~13% RH increase) and its effect became gradually reduced at higher speeds (~5% RH increase). The compressor tested at City, University of London was operated between 3 and 15 bar delivery pressure providing airflow of 2.4 -3 m3/hour. Relative humidity of the outlet air was found to be higher than the inlet air for speed and air mass flow values below 2300rpm and 68g/s respectively. Above 2300rpm, RH_{out} became lower than RH_{in} as the amount of injected water was not enough to compensate for the continuous increase of temperature. Therefore, for high operating speeds, more water injection was required to prevent supplying dry air to the fuel cell stacks. The evaporation rate was increased almost three times, as the operating speed increased from 1500rpm to 3000rpm, largely because of the increase of air mass flow rate. Yang et al (2016) have reported experimental studies on a water-injected process-gas screw compressor. The optimum water-to-air mass ratio was found to be 2–3 lit/m^3. Hanjalic and Stošić (1997) and Stošić et al (2005), have presented rotor profile generation and numerical model for thermodynamic simulation and design optimization. On an oil injected compressor test case, it was found that the temperature of the oil closely follows the gas temperature during the compressor cycle, except for extremely large oil droplet sizes (over 0.5 mm). In Li et al (2009), a thermodynamic model of the working process of water-injection twin screw compressor based on the equations of conservation of mass and energy has been presented. The two phase leakage flow through the internal leakage paths was based on the homogeneous fluid equations. Measurements of performance on a compressor with 3000 rpm and the range of water flow rate from 80 lph to 200 lph has been reported. Additional power required for water injection was less than 3.0% of the indicated power of the compressor. Discharge temperature in the range of 37 – 65 C could be achieved with water injection. A full Eulerian-Eulerian multiphase CFD analysis for oil flooded twin screw compressors has been reported in Rane et al (2016). A structured numerical mesh which can represent all moving parts of the compressor in a single numerical domain was generated by SCORG (Kovačević, 2005, Kovačević et al, 2007, Rane, 2015, Rane and Kovačević, 2017). In this study it was shown that the oil phase strongly interacts with gas phase. The heat transfer rates were calculated by specification of an interfacial area estimate and local Nusselt number. The results showed an accumulation of oil phase in the tips of the rotor lobes leading edges and also heavy flooding in the interlobe gaps. An interaction of the oil injection stream with lobes was qualitatively presented. In the current study the same framework has been used to model air and water-liquid two phase flow with an addition of the empirical form of the Lee model (Lee, 1979) for evaporation effect.

The objective of the present analysis was to estimate the temperature distribution inside the compressor, identify non-uniformity and provide data to estimate thermal deformations due to high temperatures. CFD model was used to calculate four different operating conditions with gradually increasing water content. The analysis indicates that with an increased amount of water injection into the compression chamber it is possible to control the gas discharge temperature in the limits of 200 degC which was assumed safe temperature for bearing and seal operation.

In the Eulerian-Eulerian approach of multiphase modelling, the primary and secondary phases are treated as interpenetrating continua. Phasic volume fraction α_q represents the volume of a computational cell occupied by q^{th} phase and the conservation transport equations of mass, momentum, energy and other scalars are satisfied by each phase individually. The equations are presented below.

Conservation of mass:

Continuity equation for the q^{th} phase is

$$\frac{\partial}{\partial t}\alpha_q\rho_q + div\left(\alpha_q\rho_q\vec{V}_q\right) = \sum_{p=1}^{n}\left(\dot{m}_{pq} - \dot{m}_{qp}\right) + S_q \tag{1}$$

Here, $\vec{V}_q$ is the velocity of phase q and has three Cartesian components. $\dot{m}_{pq}$ is the mass transfer term from p^{th} phase to q^{th} phase. $\dot{m}_{qp}$ is the mass transfer term from q^{th} phase to p^{th} phase. These terms will exist in situations such as evaporation and condensation phase change. S_q is any additional mass source for the phase q.

Conservation of momentum:

Momentum conservation for phase q is

$$\frac{\partial}{\partial t}\left(\alpha_q\rho_q\vec{V}_q\right) + div\left(\alpha_q\rho_q\vec{V}_q\vec{V}_q\right) = -\alpha_q grad(p) + div\,\bar{\bar{\tau}}_q + \alpha_q\rho_q\vec{g} + \sum_{p=1}^{n}\left(\vec{R}_{pq} + \dot{m}_{pq}\vec{V}_{pq} - \dot{m}_{qp}\vec{V}_{qp}\right) + \sum\vec{F}_q \tag{2}$$

$$\bar{\bar{\tau}}_q = \alpha_q\mu_q\left(\text{grad}\vec{V}_q + \text{grad}\vec{V}_q^{\,T}\right) + \alpha_q\left(\lambda_q - \frac{2}{3}\mu_q\right)div(\vec{V}_q\,\bar{\bar{I}})$$

Where, $\bar{\bar{\tau}}_q$ is the q^{th} phase stress-strain tensor with components that are function of shear and bulk viscosity. p is the pressure shared by all phases, μ_q and λ_q are the shear and bulk viscosity of phase q. $\sum\vec{F}_q$ represents all external body

forces such as lift, virtual mass, turbulent dispersion etc. $\vec{R}_{pq}$ is the interaction force between phases such as drag and interphase momentum exchange. $\vec{V}_{pq}$ and $\vec{V}_{qp}$ are the interphase velocities.

Conservation of energy:

Enthalpy conservation equation for phase q is

$$\frac{\partial}{\partial t}\left(\alpha_q \rho_q h_q\right) + div\left(\alpha_q \rho_q h_q \vec{V}_q\right) = \alpha_q \frac{dp_q}{dt} + \bar{\bar{\tau}}_q : \text{grad}\vec{V}_q - grad\vec{q}_q + S_q + \sum_{p=1}^{n}\left(Q_{pq} + \dot{m}_{pq}h_{pq} - \dot{m}_{qp}h_{qp}\right) \quad (3)$$

$$Q_{pq} = \text{ħ}_{pq} A_i \left(T_p - T_q\right) \text{ and } \text{ħ}_{pq} = \frac{k_q Nu_p}{d_p}$$

Here, h_q is the specific enthalpy of phase q. $\vec{q}_q$ is heat flux, S_q is enthalpy source, Q_{pq} is the intensity of heat exchange between phases p and q. h_{pq} is the interphase enthalpy i.e. vapour enthalpy is case of evaporation. ħ_{pq} is the heat transfer coefficient at the phasic interface, k_q is the thermal conductivity of phase q , Nu_p is Nusselt number and d_p is the vapour bubble diameter of phase p.

2. WATER EVAPORATION MODEL

Evaporation inside compression chamber has two important physical effects, one is that the latent heat of evaporating water is absorbed by gas which lowers the gas temperature and water changes state to vapour. Few models are presented in this paper that can be used alongside the CFD Eulerian multiphase framework in order to define the phasic mass and energy transfer source terms resulting due to the evaporation-condensation phase change phenomena.

2.1 Lee Model

Lee (1979) has proposed a mechanistic evaporation-condensation model that defines the phase change mass transfer source term using a time scale coefficient. The interphase mass transfer in equations (1, 2 and 3) are defined as,

If $T_w > T_{sat}$ (Evaporation),

$$\dot{m}_{pq} = \dot{m}_{wv} = C_e\, \alpha_w \rho_w \left(\frac{T_w - T_{sat}}{T_{sat}}\right) \quad (4)$$

If $T_v < T_{sat}$ (Condensation),

$$\dot{m}_{qp} = \dot{m}_{vw} = C_c\, \alpha_v \rho_v \left(\frac{T_{sat} - T_v}{T_{sat}}\right) \quad (5)$$

Note that $\dot{m}_{wv} \neq \dot{m}_{vw}$

C_e and C_c are the time scale coefficient (1/sec units), sub-scripts w and v correspond to water liquid and vapour phases respectively. T_w is water-liquid temperature, T_{sat} is the saturation temperature at pressure $\mathscr{p}$, T_v is the water-vapour temperature. In the case of air compression system with water evaporation, the pressure $\mathscr{p}$ should be taken as the vapour partial pressure $\widehat{\mathscr{p}}$.

Corresponding to this interphase mass transfer, the interphase enthalpy transfer in equation (3) is defined as,

$$Q_{pq} = Q_{wv} = \dot{m}_{wv} \cdot L \quad (6)$$

L is the latent heat due to phase change.

For a given process or machine where phase change is taking place, the time scale coefficients need to be adjusted so as to get expected phase change results. In general the coefficients are specified as 0.1 (Lee, 1979) but condensation coefficient can be high as condensation is a relatively slower process.

2.2 Thermal Phase Change Model

Unlike the Lee model, the Thermal phase change model defines the mass transfer rates entirely based on the interphase heat transfer and overall heat balance at the phasic interface. No adjustment coefficients are required apart from the solver relaxation factors for stability of the numerical solution due to mass transfer sources.

At the water-liquid and water-vapour interface heat balance gives

$$Q_w + Q_v = 0$$

From the interface to water-liquid phase,

$$Q_w = \mathfrak{h}_w A_i (T_{sat} - T_w) - \dot{m}_{wv} \cdot H_{ws}$$

From the interface to water-vapour phase,

$$Q_v = \mathfrak{h}_v A_i (T_{sat} - T_v) + \dot{m}_{wv} \cdot H_{vs}$$

Subscript s is selected depending on evaporation or condensation

$$\mathfrak{h}_w A_i (T_{sat} - T_w) - \dot{m}_{wv} \cdot H_{ws} + \mathfrak{h}_v A_i (T_{sat} - T_v) + \dot{m}_{wv} \cdot H_{vs} = 0 \quad (7)$$

$$\dot{m}_{wv} = \frac{\mathfrak{h}_w A_i (T_{sat} - T_w) + \mathfrak{h}_v A_i (T_{sat} - T_v)}{H_{vs} - H_{ws}}$$

The interphase mass transfer in equations (1, 2 and 3) are obtained from equation (7). Equation (8) and (9) are used to select the enthalpy for source in equation (3).

If $\dot{m}_{wv} > 0$ (Evaporation),

$$H_{ws} = H_w(T_w)$$
$$H_{vs} = H_v(T_{sat}) \quad (8)$$

If $\dot{m}_{wv} < 0$ (Condensation),

$$H_{ws} = H_w(T_{sat})$$
$$H_{vs} = H_v(T_v) \quad (9)$$

$$L = H_v(T_{sat}) - H_w(T_{sat}) \quad (10)$$

As seen from equation (7), the heat transfer coefficients $\mathfrak{h}_w$, $\mathfrak{h}_v$ and the interfacial area A_i must be determined in the thermal phase change model. These inputs are very difficult to be prescribed a priori. Also as the phase change progresses, the coefficients and areas can vary by a large extent. The advantage with Lee model described in section 2.1 is that these inputs are not required to initiate mass transfer.

2.3 Simplified Evaporation Model for water injected air compression

In the case of air compression with water evaporation, air is the primary phase of interest with very small quantity of water injection. Water-liquid was the secondary phase that needs to be considered not only for its effect of heat transfer with air but also for its sealing effect in the leakage gaps. As such equations for air and water-liquid two phase flow are solved. Evaporation of water-liquid to water-vapour in this process is a secondary effect and in order to reduce computational effort, the full conservation transport equations for water-vapour are not solved.

An empirical form of the Lee model has been used in the present study. It is assumed that during the entire compression process from suction pressure to discharge pressure, the secondary phase water-liquid changes to water-vapour only when its temperature exceeds the saturation temperature at discharge pressure. Such high temperatures can occur inside the compression chamber due to the heat addition of compression and reheating of leakage gas. An internal over-compression is another possible contributor. Another crude assumption is that the phase change is unidirectional i.e. only evaporation occurs and no condensation. It is anticipated that condensation, if it occurs, will only happen in the discharge pipe and not in the compression chamber where the continuous heat addition occurs. As discharge piping is not a part of the computational domain, condensation can be ignored. Once the water-liquid is evaporated it is artificially removed from the domain. The entire enthalpy of evaporation is extracted from the primary phase air and the secondary phase water-liquid resulting into their cooling. Air and water-liquid carry a complete energy and momentum transfer as defined in equations (2) and (3).

In the empirical form the evaporation mass transfer rate in equation (1, 2 and 3) for water-liquid phase is

If $T_w > T_{sat,p\_discharge}$ (Evaporation),

$$\dot{m}_{wv} = C_e \, \alpha_w \rho_w \left(\frac{T_w - T_{sat,\hat{p}}}{T_{sat,\hat{p}}} \right) \quad \text{- LEE Model} \quad (11)$$

$$\dot{m}_{wv} = -C_e' \, \alpha_w \rho_w \quad \text{- Empirical form}$$

Such that, $T_w \gg T_{sat,\hat{p}}$

$$C_e' = C_e \left(\frac{T_w - T_{sat,\hat{p}}}{T_{sat,\hat{p}}} \right) = \frac{1}{\Delta t}$$

Δt is the solver time step size.

The enthalpy source in equation 3 applied for air phase is defined as

$$Q_{va} = -\dot{m}_{wv} \cdot L \tag{12}$$

L is the latent heat due to evaporation at discharge pressure. Such an empirical model also enables the use of constant thermodynamic properties for the water-liquid in the calculations.

3. WATER CALCULATION

The water injected compressor was designed to operate between atmospheric suction pressure and a delivery pressure close to 11.0 bar absolute. It was desirable to inject a quantity of water that is just sufficient to evaporate and saturate the air at delivery conditions. Any amount of water lower than this will result into insufficient cooling of the gas with water exiting as superheated vapour. On the other side, any excess of water will accumulate in the compressor system similar to an oil flooded compressor requiring a downstream condenser. This is also not favourable option for bearings and rotors. The quantity of water required to produce saturated air depends on the initial humidity, temperature and the compression work added to reach the delivery pressure. The delivery temperature will depend on the saturation temperature at delivery pressure. The saturation pressure is a function of water temperature. As the temperature of water increases, the number of molecules transitioning into a vapour also increase, thereby increasing the vapour pressure. At a given temperature and saturation condition there is equilibrium between the molecules transitioning into vapour and vice-versa. Equations used to relate the saturation vapour pressure and temperature are available in literature (Griffith and Keller, 1965). Equation (13) by Steltz and Silvestri (1958) which relates the pressure of saturated steam to temperature is used in the present work.

$$\log_{10}\frac{p_c}{p_{sat}} = \frac{x}{T_k}\left(\frac{a + bx + cx^3}{1 + dx}\right) \tag{13}$$

Where,

$a = 3.2437814$,
$b = 5.86826 \times 10^{-3}$,
$c = 1.1702379 \times 10^{-8}$,
$d = 2.1878462 \times 10^{-3}$,

$p_{sat} = saturation\ pressure\ (atm)$,
$T_k = temperature(K)$,
$p_c = critical\ pressure = 218.167\ atm$
$T_c = critical\ temperature = 647.27\ K$,
$x = T_c - T_k$

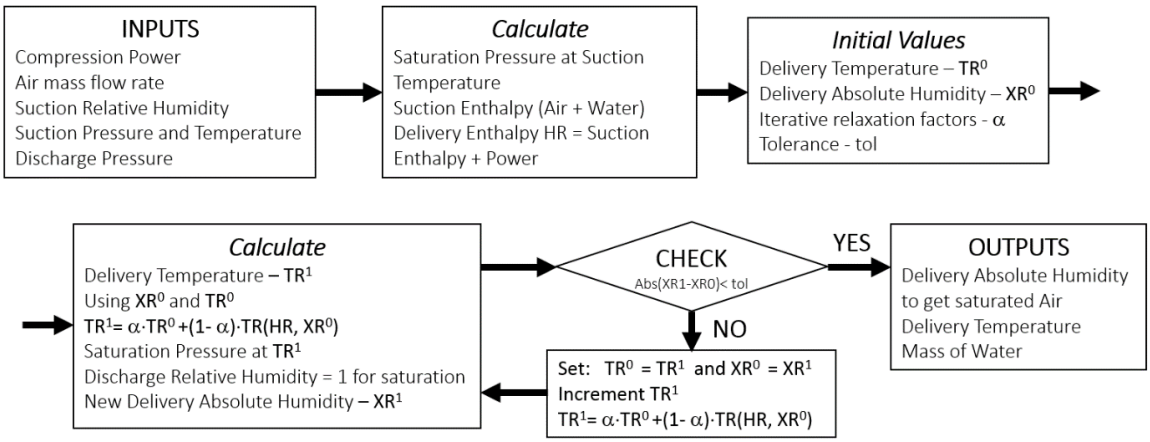

Figure 1: Flow chart of the water mass calculator

From psychrometric relations,

Absolute Humidity (kg of water-vapour per kg of air)

$$XR = \frac{0.622 \cdot p_v}{p - p_v} \tag{14}$$

Relative Humidity

$$RH = \frac{p_v}{p_{sat}} \tag{15}$$

p_v is the vapour pressure and p_{sat} is the saturation vapour pressure at temperature T_k. At saturation, $RH = 1$.

Using equations (13, 14 and 15) an iterative water calculation procedure was used that starts with an initial delivery temperature and humidity conditions and using successive increment estimates the mass of water required to produce saturated air at the delivery pressure. Figure 1 presents a flow chart of the water calculator.
Analysis of the amount of water required for a specified quantity of air and suction conditions indicates that for the air mass flow rate considered in this study (Design air flow value could not be disclosed), it is possible to achieve a delivery temperature in the range of 100 – 160 degC at 11.0 bar discharge pressure for a range of compression power requirements. A range of compression power between 15 – 50 kW originates from an estimated adiabatic efficiency of the compressor which could vary from 25 to 85%. The water calculator is independent of the type of the compressor used.

3.1 Water mass requirement

Figure 2 presents the quantity of water in kg/min required when the suction is at atmospheric pressure with relative humidity 3%. There is proportional increment in water mass requirement from ~0.2 kg/min at 10kW power to ~1.2 kg/min at 60kW. Increasing suction temperature from 10 degC to 25 degC resulted in a small increase in required water mass flow for saturation.

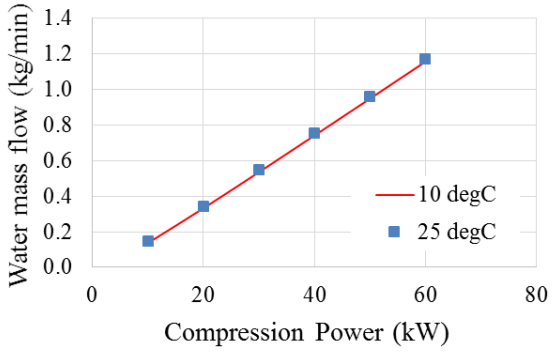

Figure 2: Water mass flow required for saturation of air at 11.0bara discharge

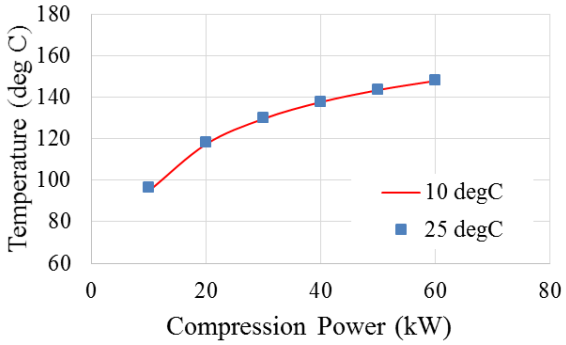

Figure 3: Saturation temperature of air at 11.0bara discharge

Figure 3 presents the estimate of delivery temperature. From 10 kW to 60 kW the delivery temperature with saturation condition can vary from 100 degC to 150 degC. Increasing suction temperature from 10 degC to 25 degC resulted in very close delivery temperatures as this was compensated by an incremental evaporated water mass.

3.2 Influence of suction humidity

Figure 4 shows a relative difference in water mass flow required for saturation when the suction humidity is increased from 3% to 15%. Values at 10 degC are used as reference. At 10 kW power a 2%, 4% and 8% higher water mass is required to produce saturation with 15% RH, 25 degC 3% RH and 25 degC 15% RH suction condition respectively. This incremental value drops to a very low percentage < 1% at 60 kW power.

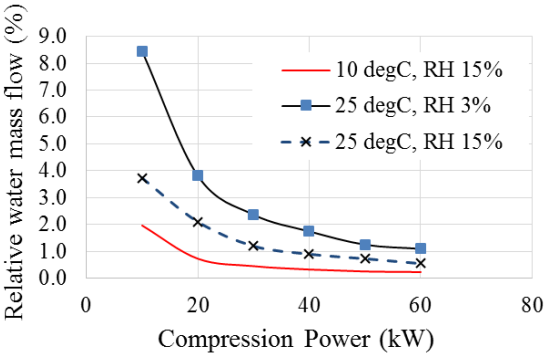

Figure 4: Required water mass flow for saturation conditions at discharge relative to 3% RH

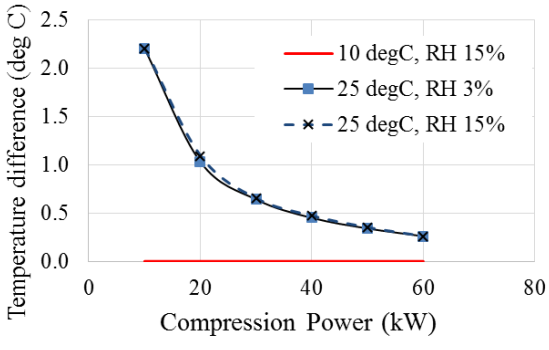

Figure 5: Delivery temperature variation relative to 3% RH

Figure 5 shows the delivery temperatures when the suction humidity is increased indicating that there will be no difference providing sufficient amount of water is injected. These results indicate that the effectiveness of cooling the compressed air reduces with the increase in the suction temperature. The increase in relative humidity and temperature at suction can be compensated by varying the water mass flow rate to produce the same delivery temperature.
An important consideration when using these results is that in the real compression chamber the injected water will have a limited residence time available for heat transfer and evaporation and before the entire injected water mass is evaporated, it could leave the compression chamber thereby producing higher temperatures then predicted by the water calculator here. The water calculator procedure estimates mass of water as per unit mass of air but does not account for transient physical behaviour of the compression process.

4. CFD MODEL OF WATER INJECTED TWIN SCREW COMPRESSOR

Description of typical CFD modelling for twin screw compressors in presented in detail in Rane (2015), Rane and Kovačević (2017). The whole working domain of the compressor is split into four main sub-domains namely rotor domain, suction port, discharge end leakage gap and discharge port. All sub-domains are connected in the solver by non-conformal interfaces. The grid for the rotor domain is generated using SCORG while grids for all stationary domains are obtained using ANSYS meshing. ANSYS CFX solver is used for the calculations in this study. An inhomogeneous formulation as described by equations (1, 2 and 3) treats momentum transport for each phase separately and can account for high slip conditions. Evaporation of water-liquid phase is defined as per equation (11) and $T_{sat,\hat{p}} = 184.06$ C is specified with latent heat $L = 1998.55$ kJ/kg in equation (12) corresponding to 11.0 bar delivery pressure. Four cases were calculated in this study. The operating conditions are as shown in Table 1. As observed from initial calculations and also based on Ous et al (2012) experiments, it was required to increase the injected water mass compared to that estimated by saturation water calculator in order to achieve sufficient cooling.

Table 1: CFD cases evaluated and resultant delivery temperature at 11.0 bar

	Speed (rpm)	Water (kg/sec)	Remark	Average Discharge Temperature (C)
Case1	6000	0.018	2x – twice the saturation mass	325
Case2	4500	0.009	Saturation Mass - x	262
Case3	4500	0.045	5x – five times the saturation mass	205
Case4	6000	0.090	10x – ten times the saturation mass	187

Table 2: Fluid properties

Property	**Air**	**Water Liquid**	**Units**
Density	Ideal Gas	997.0	kg m^{-3}
Dynamic Viscosity	1.83e^{-05}	8.889e^{-04}	kg m^{-1} s^{-1}
Thermal Conductivity	2.61e^{-02}	0.6069	Wm^{-1} K^{-1}
Specific heat capacity	1004.4	4181.7	J kg^{-1} K^{-1}

Properties of fluids used as phases in the multiphase calculation are defined in Table 2 with air as the primary phase and water-liquid as the secondary phase. Pressure boundary conditions were specified at the suction and discharge. Solver parameters were set at higher stability conditions. A number of iterations were performed and different settings tested to determine the combination that works robustly for the mesh and flow conditions. SST k-Omega turbulence model was applied.

5. RESULTS AND DISCUSSION

Results from CFD analysis are presented in this section. They reflect a state when full 11.0 bar discharge pressure has been reached in the discharge port and 1-2 cycles of calculation were performed at these operating conditions. The cycle averaged temperature data were collected during the calculation.

5.1 Internal pressure and power

Figure 6 shows the pressure in the compression chamber as function of the main rotor angle of rotation for Case1 at 6000 rpm and 0.018 Kg/sec water mass flow rate. Both air and water inside the chamber are at the same pressure. Because of the high under-compression which can be observed by the steep pressure rise at 350 degree rotor angle, a strong pressure pulse is generated in the discharge port. Figure 7 shows the variation of indicated power in one compression cycle for Case1 at 6000 rpm and 0.018 Kg/sec water mass flow rate condition and Case2 at 4500 rpm and 0.009 Kg/sec water mass flow rate condition. The average indicated power at 6000rpm is 21.0 kW and at 4500rpm it is 15.0 kW. The average torque on the main rotor is close to 30.0 Nm while that on the gate rotor is close to 3.69

Nm. The direction of gate rotor torque is opposite to that of the main rotor. Since all the cases 1 to 4 have been calculated at 11.0 bar discharge pressure the resultant rotor torque is in the similar range.

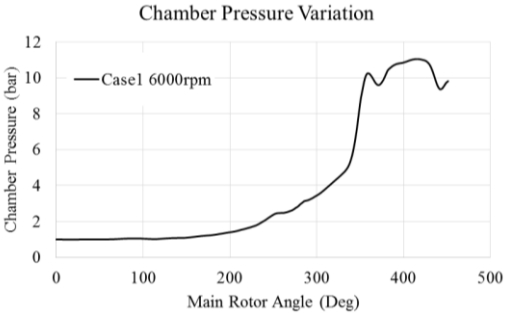

Figure 6: Internal chamber pressure variation during a cycle

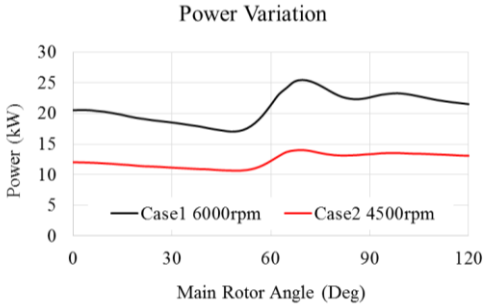

Figure 7: Compression power variation during a cycle

5.2 Air temperature

If water was not injected in the compressor, the temperature of air would have exceeded 380 degC at 11.0 bar discharge pressure. In the cases analysed, water has been injected at 10 degC. Table 1 shows the average air temperature at the discharge pressure in the four cases. It can be observed that for a low water mass flow rate of 0.009 Kg/sec the cooling effect is stronger in Case 2 at 4500 rpm compared to Case 1 at 6000rpm which has 2x water mass flow compared to Case 2.

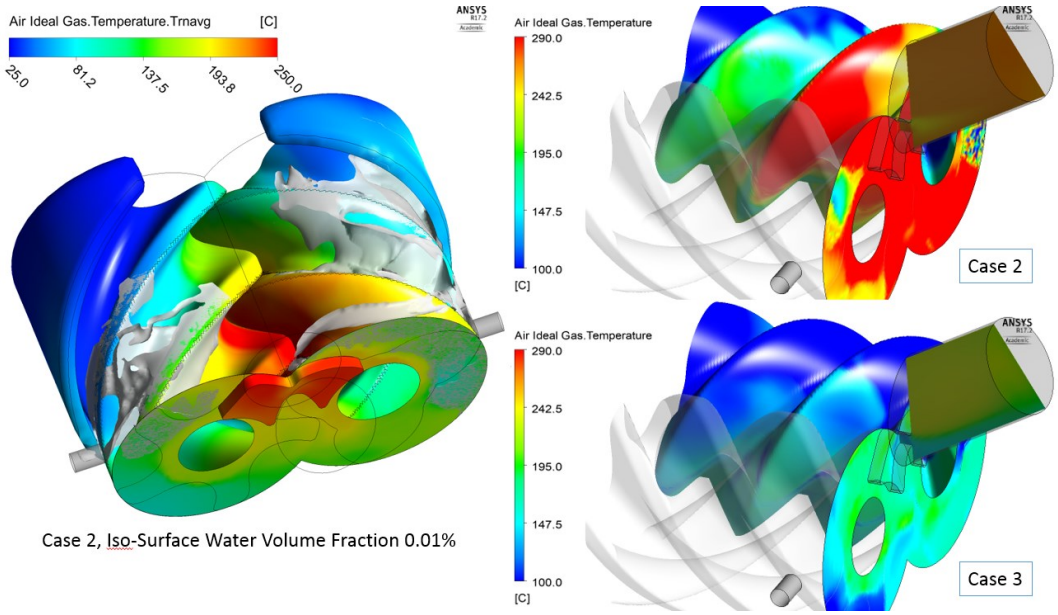

Figure 8: Cycle average Air temperature distribution with an Iso-surface of liquid water

The water mass of 0.009 Kg/sec was determined so as to achieve saturated air at the exit with power dissipation of approximately 30 kW. But these estimates did not account for transient affects. CFD calculation has therefore resulted in higher than saturation exit temperatures. Additionally the leakage of gas during compression adds to the accumulation of energy in the compression chamber which further raises the gas temperature. Cases 2 and 4 were designed such that the mass flow rate of water is 5x and 10x of the saturation mass of Case 2 respectively with the aim of achieving a discharge temperature lower than 200 degC. The limit of 200 degC is due to the maximum temperature that the compressor oil used for bearings and seals can withstand during operation. It can be observed from Table 1 that the temperature of 205 degC is achieved at 4500 rpm and 187 degC is achieved at 6000rpm with increased mass flow of water. Figure 8 shows the air temperature inside the compressor. An iso-surface generated with liquid volume fraction of 0.01% is also shown in the figure. The temperature in the suction port is lower on the gate rotor side, but on the main rotor side shows higher air temperature. This indicates that the leakage is higher from

the tip of the main rotor as compared to the gate rotor and also that the cooling is more effective on the gate rotor side as compared to the main rotors side for the same mass of injected water. The temperature on the gate rotor is higher than on the main rotor close to the discharge port. Water-liquid is observed in the region where air temperature is below the saturation temperature at 11.0 bar. Evaporation effect is visible in the compression chamber opened to the discharge port and also in the discharge port i.e. no liquid water is present here. In comparison to Case 2, Case3 showed about 50 degC lower cycle average temperature.

5.3 Evaporation effect

Figure 9 shows the vapour formation and cooling of air. Figure 9a shows the air temperature distribution on the main rotor surface, in the end leakage and in a plane through the discharge port. Figure 9b shows the region where liquid water is converted to vapour. Figure 9c shows the distribution of liquid water on the main rotor surface and Figure 9d shows the latent heat being removed from air in regions where evaporation is active. The air temperature and presence of liquid water can be correlated to the regions of vapour formation and heat extraction in this figure. Due to very low mass of water - 0.009 Kg/sec in this Case 2 the local air temperature reaches to about 290 C. In Case 3 which had 5 times higher mass injection as compared to Case 2 the peak air temperature dropped to below 200 C as shown in Figure 8.

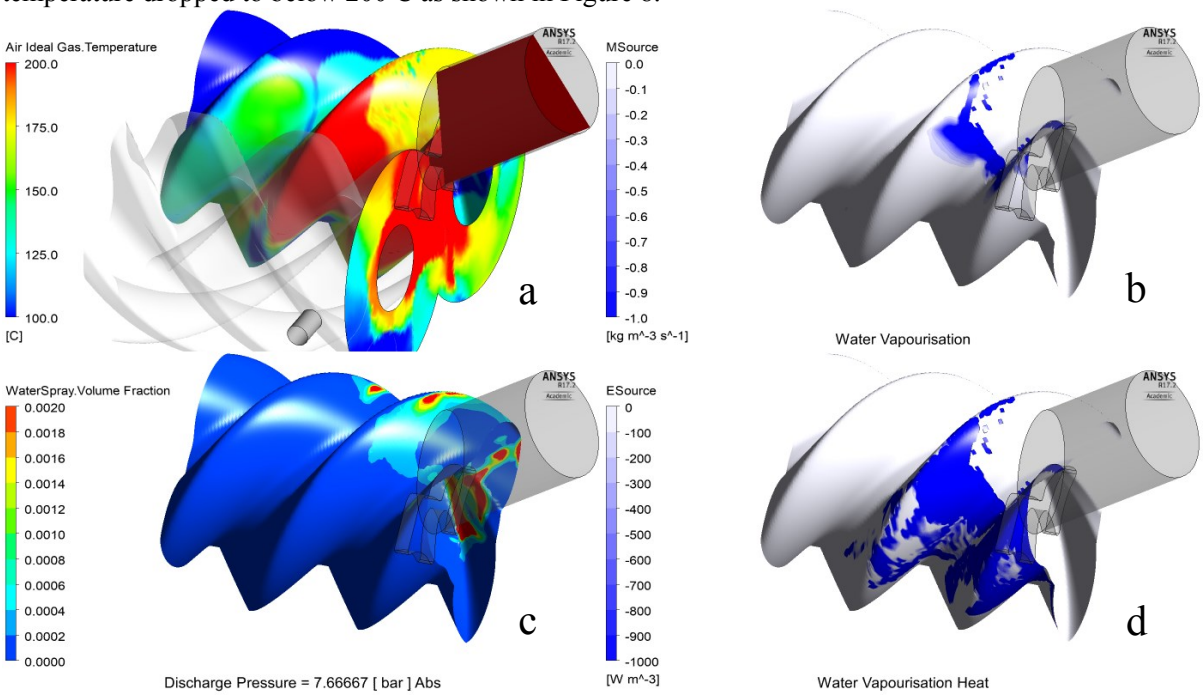

Figure 9: Visualization of Case 2, a) Air temperature distribution, b) Regions of water evaporation, c) Liquid water distribution and d) Regions of liquid latent heat transfer

6. CONCLUSIONS

Objective of the CFD analysis was to study the feasibility of the compressor to operate at 11.0 bar discharge pressure with a very low amount of water injection, just enough to provide cooling. A water calculation procedure was used to estimate the mass of water required to produce saturated air at delivery pressure. A multiphase CFD model was set up to solve air and water-liquid flow along with the simplified evaporation model to account for the latent heat of vaporisation. Analysis of the test cases indicate the following:

- Results show higher cooling at 4500 rpm than at 6000 rpm for the same water mass flow rate. Total mass of water injected and its residence time in the compression chamber is higher at lower speed resulting in a greater heat transfer and cooling. At 4500 rpm the compression power is lower than at 6000 rpm. Therefore the same mass of water will provide higher cooling at lower speeds.
- When water mass required just for saturation is injected, the exit temperature exceeds 300 C. By injecting five times higher water mass flow, the cycle average temperature close to 200 C could be achieved.

- In this compressor design, the water cooling effect was higher on the Gate rotor side due to earlier injection. But the peak temperature close to the discharge port is higher on the Gate rotor side. An increase in the water injection on the main rotor side can help to achieve better temperature uniformity.
- Tip Leakage is higher on the main rotor side and this results in non-uniform temperature on the housing.

In future, a design with water injection in the suction port can be considered. It can help in cooling the intake air, provide rotor film formation that can help cooling and lubrication of the rotors. In terms of CFD modelling a three fluid calculation with full evaporation-condensation phase change formulation could provide better accuracy in the estimate of delivery temperature and humidity.

REFERENCES

ANSYS CFX User Guide (2017).

Chamoun, M., Rulliere, R., Haberschill, P. & Peureux, J. L. (2013). Modelica-based modeling and simulation of a twin screw compressor for heat pump applications. Appl. Therm. Eng. 58, 479–489.

Griffith, W. L., & Keller, R. M. (1965). SALINE: A Fortran Computer Program for the Process Design of saline water conversion plants using the Multi-Stage, Flash-Evaporation Process. United States: N. p., 1965.

Hanjalic, K., Stošić N. (1997). Development and optimization of screw machines with a simulation model, Part II: Thermodynamic performance simulation and optimization. *ASME Trans*. J. Fluids Eng. 119, 659–670.

Kovačević, A. (2005). Boundary Adaptation in Grid Generation for CFD Analysis of Screw Compressors, *Int. J. Numer. Methods Eng*., 64(3): 401-426.

Kovačević, A., Stošić, N. & Smith, I. K. (2007). *Screw compressors - Three dimensional computational fluid dynamics and solid fluid interaction*, ISBN 3-540-36302-5, Springer-Verlag Berlin Heidelberg New York.

Kovačević, A, Rane S. (2017). Algebraic generation of single domain computational grid for twin screw machines Part II – Validation, Advances in Engineering Software, 107, pp., doi: 10.1016/j.advengsoft.2017.03.001

Lee, W. H. (1979). A Pressure Iteration Scheme for Two-Phase Modelling. *Technical Report LA-UR79-975*. Los Alamos Scientific Laboratory, Los Alamos, New Mexico.

Li, J., Wu, H., Wang, B., Xing, Z. & Shu, P. (2009). Research on the performance of water-injection twin screw compressor. Appl. Therm. Eng. 29, 3401–3408.

Ous, T., Mujic, E. & Stošić, N. (2012). Experimental investigation on water-injected twin-screw compressor for fuel cell humidification. *Proc of the IMechE*, Part C: Journal of Mechanical Engineering Science. 226. 2925-2932.

Rane, S. (2015). Grid Generation and CFD analysis of variable Geometry Screw Machines, PhD thesis, City, University of London, London.

Rane, S., Kovačević, A. & Stošić, N. (2016). CFD Analysis of Oil Flooded Twin Screw Compressors. Int. Compressor Eng. Conference, Purdue. Paper 2392.

Rane, S., Kovačević, A. (2017). Algebraic generation of single domain computational grid for twin screw machines. Part I. Implementation, Advances in Engineering Software, 107, pp. 38-50.

Sangfors, B. (1998). Computer Simulation of Effects from Injection of Different Liquids in Screw Compressors. Int. Compressor Eng. Conference, Purdue. Paper 1305.

SCORG Help Manual (2017).

Shen, J., Xing, Z., Zhang, K., He, Z., & Wang, X. (2016). Development of a water-injected twin-screw compressor for mechanical vapor compression desalination systems. Appl. Therm. Eng. 95, 125–135.

Steltz, W. G., Silvestri, G. J. (1958). The formulation of steam properties for digital computer application. *Transactions of the ASME*, 80 , 967 – 973.

Stošić, N., Smith, I. K. & Kovačević, A. (2004). *Estimation and control of heat transfer in screw compressor rotors*, Proceedings of the 2004 ASME International Mechanical Engineering Congress and Exposition, November 14-19, 2004, Anaheim, CA

Stošić, N., Smith, I. K. & Kovačević, A. (2005). *Screw Compressors: Mathematical Modelling and Performance Calculation*, Springer Verlag, Berlin, ISBN: 3-540-24275-9.

Yang, Q., Liu, C., Zhang, Q., Liu, G., Zhao, Y. & Li, L. (2016). Experimental investigation of the water-injected process-gas screw compressor. *Proc of the IMechE*, Part E: Journal of Process Mechanical Engineering. 232.

ACKNOWLEDGEMENT

This research was supported by Jäcklin GmbH, Augsburg. Authors would like to thank Ms Julia Jäcklin, Mr Jürgen Jäcklin and Mr Andreas Korner from Jäcklin GmbH for their technical inputs during the work.